



**HAL**  
open science

# On the local corrosion in a thin layer of electrolyte separating two materials: specific aspects and their contribution to pad-to-disk stiction in automobile brake system

Rafik Tigane, Denis Bauwens, Olivier Hude, Suzanne Joiret, Michel Keddam, Mireille Turmine, Vincent Vivier

## ► To cite this version:

Rafik Tigane, Denis Bauwens, Olivier Hude, Suzanne Joiret, Michel Keddam, et al.. On the local corrosion in a thin layer of electrolyte separating two materials: specific aspects and their contribution to pad-to-disk stiction in automobile brake system. *Journal of Solid State Electrochemistry*, 2021, 25 (3), pp.895-904. 10.1007/s10008-020-04867-w . hal-03160287

**HAL Id: hal-03160287**

**<https://hal.science/hal-03160287>**

Submitted on 5 Mar 2021

**HAL** is a multi-disciplinary open access archive for the deposit and dissemination of scientific research documents, whether they are published or not. The documents may come from teaching and research institutions in France or abroad, or from public or private research centers.

L'archive ouverte pluridisciplinaire **HAL**, est destinée au dépôt et à la diffusion de documents scientifiques de niveau recherche, publiés ou non, émanant des établissements d'enseignement et de recherche français ou étrangers, des laboratoires publics ou privés.

[Click here to view linked References](#)

# On the local corrosion in a thin layer of electrolyte separating two materials. Specific aspects and their contribution to pad-to-disk stiction in automobile brake system

**Rafik TIGANE,<sup>a,b</sup> Denis BAUWENS,<sup>a</sup> Olivier HUDE,<sup>a</sup> Suzanne JOIRET,<sup>b</sup>  
Michel KEDDAM,<sup>b</sup> Mireille TURMINE,<sup>b,\*</sup> Vincent VIVIER<sup>b</sup>**

<sup>a</sup> Hitachi Automotive Systems, 126 rue de Stalingrad, F-93705, Drancy, France

<sup>b</sup> Sorbonne Université, CNRS, Laboratoire Interfaces et Systèmes Electrochimiques (LISE), 4 place Jussieu, F-75005, Paris, France

## Abstract

The stiction phenomenon which results in the adhesion of the brake pad to the disc brake of a vehicle has been investigated from a corrosion point of view. Asbestos-free organic pad that contains copper associated with a cast iron disc was investigated and compared to a model system which consisted in a ceramic pad (chemically inert) associated with the same cast iron disc. The whole system was described as a thin-layer-cell of electrolyte and was studied using different electrochemical methods including polarization curves and impedance spectroscopy. The influence of the cell geometry was pointed out, but the corrosion of the system is enhanced due to the presence of copper in the pad. Indeed, the copper dissolves from the pad and redeposits on the disc. This was confirmed by scanning electron microscopy observations and Raman spectroscopy. A mechanism taking into account the thin-layer geometry was then proposed to account for the role of metallic additive (in this case copper) on the corrosion of the disc.

## Keywords

Thin-layer electrochemistry; Electrochemical impedance spectroscopy; Copper dissolution; Galvanic corrosion

*\*Corresponding author: mireille.turmine@sorbonne-universite.fr*

# 1. Introduction

Vehicles are equipped with braking systems to slow it down or keep it static [1-4]. The disk-brake consists mainly of a disc made of a graphite cast iron and a pad formulated with various friction materials, including asbestos-free organic pads, semi-metallic pads and low-metal content pads [5]. It has been observed that after a long period of parking, the pad can stick strongly to the disc, especially in winter conditions, making it difficult to release the parking brake. In some cases, the tangential force exerted when starting the vehicle is far from being sufficient. This phenomenon, commonly referred to as stiction, occurs unexpectedly and may cause a temporary immobilization of the vehicle and / or the pad material to tear off.

Although stiction is a common problem in the automotive industry, to date it is poorly documented and remains largely unexplained [6-8]. However, it has been reported that during stiction, iron oxide at the pad/disc interface is systematically observed and that, consequently, the stiction phenomenon would result in some way from the corrosion of the brake disc [8]. Indeed, this problem involves the same ingredients as crevice corrosion [9-13], but it cannot be reduced to a crevice since the stiction is strongly dependent on the pad formulation.

A likely explanation lies in the forces generated by the growth of disc corrosion products resulting, at constant free volume, in a strong bond between disc and pad. These huge forces have been considered in stress corrosion cracking [14], provoking the failure of reinforced concrete by expansion of the corrosion products of the steel bars. In a more quantitative way, the forces developed by salt crystallisation and the associated weathering damages in porous artefacts have been thoroughly investigated [15,16]. Wedging actions on stainless steels associated to corrosion products are also interpreted by similar effects [14]. Pressures up to hundred MPa are predicted from thermodynamics and experimentally observed while the pad-disk pressure during braking is 1-10 MPa.

1  
2  
3  
4  
5  
6  
7  
8  
9  
10  
11  
12  
13  
14  
15  
16  
17  
18  
19  
20  
21  
22  
23  
24  
25  
26  
27  
28  
29  
30  
31  
32  
33  
34  
35  
36  
37  
38  
39  
40  
41  
42  
43  
44  
45  
46  
47  
48  
49  
50  
51  
52  
53  
54  
55  
56  
57  
58  
59  
60  
61  
62  
63  
64  
65

These results indeed also strongly suggest that the influence of the composition of the pad must be taken into consideration. Unfortunately, the detailed formulation and fabrication processes of the pads are not available. Nevertheless, their nominal composition usually includes binders, frictional additives, graphite, reinforcing fibers such as copper fibers, etc. in varying proportions [17,18,3,19].

In recent years, in addition to the phenomenon of friction, the study of brake disc corrosion has aroused growing interest for various reasons, including the impact of corrosion on the friction properties [20-23], the effect of brake disc corrosion on friction-induced stick-slip [24,25] and the corrosion issues that lead to material transfer from the pad to the disc [26]. In addition, for a comprehensive description of the corrosion process which can lead to stiction, a purely physico-chemical description of the phenomenon may be insufficient since the configuration of the disc/brake pad system builds a thin layer of electrolyte between the two materials, which can account for a significant part of the corrosion and stiction processes, not least because of the potential and concentration gradients that such an arrangement generates [27,28].

Based on these observations, the stiction phenomenon was studied in this work by electrochemical techniques, including electrochemical impedance spectroscopy (EIS) in combination with *ex situ* surface analysis (scanning electron microscopy and Raman microspectroscopy). It should be mentioned that to our knowledge, there is no work applying EIS to the study of stiction phenomena.

The second important point of this work is the focus on one component of the pad, namely copper. This material has an important role in the thermal transfer [29] and friction since it participates in a large extent to the formation of the transfer film and the third body [29-32].

We are clarifying a totally different mechanism of Cu transfer from pad to disk ending in single nanocrystals only compatible with growth from a soluble Cu compound [29,33].

1  
2  
3  
4  
5  
6  
7  
8  
9  
10  
11  
12  
13  
14  
15  
16  
17  
18  
19  
20  
21  
22  
23  
24  
25  
26  
27  
28  
29  
30  
31  
32  
33  
34  
35  
36  
37  
38  
39  
40  
41  
42  
43  
44  
45  
46  
47  
48  
49  
50  
51  
52  
53  
54  
55  
56  
57  
58  
59  
60  
61  
62  
63  
64  
65

In the case of stiction, it will be shown that copper can be found in the elemental composition of corrosion products observed on the surface of the iron brake disc, mainly as metallic copper but also as copper oxides. We will therefore propose a mechanism to explain how copper dissolves in the ionic solution between the disc and the pad, and then redeposits on the disc, which could speed up the corrosion of the disc by galvanic cell effect.

## 2. Experimental part

### 2.1. Materials

Three different types of brake pads (BP) were used in this work in order to, first, highlight the influence of the pad composition on the electrochemical response of the braking system (and more specifically the disc corrosion) and in a second step, to study the role of copper and particularly its dissolution and its subsequent deposit on the disc surface. For the study of the pad composition, non-asbestos organic (NAO) brake pads were used whereas ceramic pads (CPs) made of  $ZrO_2$ - $Y_2O_3$  were used as non-reactive material. The later was used to mimic the influence of the thin layer formed between pad and disc while getting free of the composition and reactivity of the pad. For investigating the influence of copper that can be encountered in NAO pads, home-made Teflon<sup>®</sup> pads (TPs) incorporating pure copper wires were used for the second part of the work. Two types of TPs were used: TP with a single copper wire and TP with five copper wires. Through-holes of 1.2 mm in diameter were drilled in the TP and 1 mm in diameter Cu wires coated with a cathaphoretic paint were sealed with an epoxy resin. All pads samples were 1.5 x 1.5 x 1.5 cm<sup>3</sup> cubic samples, and the surface area of each pad was 2.25 cm<sup>2</sup>. Regarding the disc sample, all the experiments were performed using a GG25 cast iron brake disc, the composition of which is given in Table 1. The active surface area of the disc was delimited with an adhesive PTFE mask and was 10 cm<sup>2</sup> (Fig. 1a).

1 All BP sides were covered by a thick layer of insulating paint, except for the surface in contact  
2 with the disc, as shown in Fig. 1b. Before each experiment, samples were polished with a SiC  
3 abrasive paper (P320) then rinsed with distilled water and finally dried with air.  
4  
5  
6

7 *Table 1 - Chemical composition of disc samples in weight percent (wt%).*  
8

9

Element	C	Si	Mn	S	P	Cr	Cu	Fe
% MIN	3.2	1.8	0.5	-	-	-	-	balance
% MAX	3.6	2.4	0.9	0.15	0.12	0.35	0.6	balance

10  
11  
12  
13  
14  
15  
16  
17  
18  
19

## 20 2.2. Electrochemical measurements and solutions

21

22 All the experiments were performed in a 5% NaCl solution, which was prepared freshly from  
23 high purity water (Aquadem - Veolia®) and analytical grades chemicals. Such a high chloride  
24 concentration is justified by the thin layer configuration of the system. Indeed, even if in real  
25 conditions the concentration may vary over a wide range of values, one can guess that after the  
26 evaporation of the salted water thin film on the surface of the disc, the concentrations can  
27 become very high.  
28  
29  
30  
31  
32  
33  
34  
35  
36

37 As illustrated in Fig. 2, the BP was placed on the top of disc after immersion in the NaCl solution  
38 in order to avoid trapping air between the disc and the pad. No additional force was applied to  
39 the sample (the influence of the pressure applied by the pad on the disc is not the aim of this  
40 study). All the electrochemical measurements (open-circuit potential,  $E_{oc}$ , polarization curves,  
41 EIS) on the disc were performed with a classical 3-electrode-cell configuration using a Gamry®  
42 Interface 1000E potentiostat. The electrochemical cell consisted of a glass tube clamped to the  
43 sample. The O-ring of the cell contacted the adhesive deposited on the disc, thus avoiding local  
44 (crevice) corrosion to develop at the disc/cell interface. The reference electrode was a saturated  
45 Ag/AgCl reference electrode ( $E_{Ag/AgCl} = 0.197$  V vs. SHE) and the counter-electrode was either  
46 a graphite rod or a Pt grid. Preliminary experiments were performed with and without spacers  
47  
48  
49  
50  
51  
52  
53  
54  
55  
56  
57  
58  
59  
60  
61  
62  
63  
64  
65

1 and with samples of different sizes in order to show the possibility to measure an electrical  
2 signal even when no spacer was used. It was shown that the amount of electrolyte in the as-  
3 formed thin layer was sufficient for performing the experiments.  
4  
5

6  
7 All EIS measurements have been performed in potentiostatic mode using a 10 mV (rms)  
8 amplitude for the perturbation over a frequency range spreading from 100 kHz down to 10 mHz  
9 with 10 points per frequency decades.  
10  
11

12  
13 The copper dissolution/redeposition experiments with the Teflon pad were performed by  
14 measuring the potential at open circuit of the disc sample simultaneously with those of the Cu  
15 wires with the help of National Instruments® data acquisition card connected to BNC adapter.  
16  
17 In that case, the thin layer thickness was controlled using 1 mm thick spacers along two of the  
18 four edges of the pad facing the disc (Fig. S1). This approach makes it possible to highlight the  
19 driving role of chemistry and to avoid possible electronic contact between the constructive  
20 materials of the pad and the disc.  
21  
22  
23  
24  
25  
26  
27  
28  
29  
30  
31  
32  
33  
34  
35

### 36 2.3. Sample characterization

37  
38  
39 After experiments, the electrodes were removed from solution, rinsed with ultrapure water and  
40 dried-up with air gun. Surface analyses were performed using stereo-optical microscopy  
41 (Zeiss®), scanning electron microscopy (SEM) coupled to energy-dispersive X-  
42 ray spectroscopy (EDAX) (Zeiss®). Micro Raman spectroscopy analyses were performed with  
43 a Notch filter-based spectrometer (Horiba – Jobin Yvon®), using a He-Ne laser emitting at  
44 632.8 nm and an Olympus® microscope with 50x and 100x objectives (beam size 5 and 2  $\mu$ m,  
45 respectively).  
46  
47  
48  
49  
50  
51  
52  
53  
54  
55  
56  
57  
58  
59  
60  
61  
62  
63  
64  
65

### 3. Results and discussions

#### 3.1. Electrochemical measurements

**Error! Reference source not found.** shows the evolution of the corrosion potential for the cast iron with and without a pad on the disc surface. It is worth noting that for the bare disc and for the disc with a chemically inert pad (ceramic pad), the shape of the curves is similar and tends toward the same quasi-steady-state value after 150 min of immersion in 5% NaCl solution, *i.e.*,  $E_{\text{corr}} = -0.767 \text{ V vs. Ag/AgCl}$ . When the same experiment is performed with a NAO pad that contains Cu fibers (Fig. 3a – blue curve), the corrosion potential also decreases with time to reach a higher value of corrosion potential at *ca.*  $E_{\text{corr}} = -0.707 \text{ V vs. Ag/AgCl}$ .

These experiments were carried out 6 times and have systematically led to an increase in corrosion potential between 45 and 65 mV when a NAO pad is placed on the disc.

For longer immersion times (up to 72 hours), a definitely different behaviour is evident as shown in Fig. 3b. The corrosion potential of the bare disc slowly increases whereas the corrosion potential of the disc in presence of a ceramic pad or a NAO pad tends towards  $-0.76 \text{ V vs. Ag/AgCl}$  and  $-0.78 \text{ V vs. Ag/AgCl}$ , respectively. Roughly speaking, the curves are intersecting around 15-25 h resulting in an opposite order of the OCP's with respect to the short-time ones. These differences can be attributed on the one hand to the potential distribution due to the formation of a thin layer of electrolyte between the disc and the pad, but also to a possible contribution due to the presence of copper in the pad (*vide infra*). Indeed, this purely physical explanation, which only takes into account the current and potential distributions related to the geometry of the system, must be confronted with the physico-chemistry of the system. Copper can catalyse the oxygen reduction reaction [34,35], which results in a local increase in pH in the thin layer. The limited amount of dissolved oxygen can then be compensated in this confined environment by a potential shift to more negative values allowing water reduction [36,37].

1  
2  
3  
4  
5  
6  
7  
8  
9  
10  
11  
12  
13  
14  
15  
16  
17  
18  
19  
20  
21  
22  
23  
24  
25  
26  
27  
28  
29  
30  
31  
32  
33  
34  
35  
36  
37  
38  
39  
40  
41  
42  
43  
44  
45  
46  
47  
48  
49  
50  
51  
52  
53  
54  
55  
56  
57  
58  
59  
60  
61  
62  
63  
64  
65

The polarisation curves in Fig. 4 were performed by linear potential sweep technique at 0.2 mV s<sup>-1</sup> after 150 min immersion of the samples either in absence (black curve) or in presence of a pad on the cast iron disc (red curve for a ceramic pad and blue curve for a NAO pad). These curves were obtained from the cathodic domain (starting potential at  $E_{\text{corr}} - 0.030$  V vs. Ag/AgCl). Interestingly, the slight cathodic polarisation of the electrode does not change the ranking of the corrosion potentials obtained from immersion tests (Figs. 4 & 5). Moreover, the corrosion current density can be obtained from the extrapolation of the Tafelian region of the cathodic or the anodic branch. For the latter, a sufficiently high overpotential is required in order to disregard the cathodic contribution in the low overpotential domain [38]. For the cathodic branch, the anodic contribution can be disregarded when the sizes of the electroactive domains are small when compared to the diffusion layer thickness [39,40]. For the disc alone and in the presence of the ceramic pad, the corrosion current densities are  $(0.60 \pm 0.10)$  mA cm<sup>-2</sup> and  $(0.75 \pm 0.08)$  mA cm<sup>-2</sup>, respectively. In the presence of the NAO pad, this value increases to  $(3.10 \pm 0.12)$  mA cm<sup>-2</sup>. Each type of measurements was repeated three times and the uncertainty is calculated from the deviation to the mean value. It should be noticed that the value measured in presence of the NAO pad, which is significantly higher, is converted in current density by considering the total geometric surface of the disc as the active surface, a choice which may be debatable as we shall see later. In addition, the value of the corrosion current density is difficult to determine from the anodic contribution for the disc-plus-NAO pad system. Indeed, except at high current densities no clear slope can be evidenced from the anodic branch of the current/potential curve and we have therefore chosen to discuss only the values obtained from the extrapolation of the cathodic branch to the corrosion potential. Such an evolution of the anodic current/potential curve indicates that Tafel's law alone cannot, *a priori*, depict the mechanism of dissolution of iron in the thin film of electrolyte. When the same experiments were performed after a shorter immersion time (*i.e.* 10 min – dashed curves on Fig.

1  
2  
3  
4  
5  
6  
7  
8  
9  
10  
11  
12  
13  
14  
15  
16  
17  
18  
19  
20  
21  
22  
23  
24  
25  
26  
27  
28  
29  
30  
31  
32  
33  
34  
35  
36  
37  
38  
39  
40  
41  
42  
43  
44  
45  
46  
47  
48  
49  
50  
51  
52  
53  
54  
55  
56  
57  
58  
59  
60  
61  
62  
63  
64  
65

4), the curves were similar but shifted towards more anodic potentials and with lower current densities. It can therefore be deduced that during the first few hours of immersion, a shift of the potentials towards more negative values and a noticeable acceleration of corrosion are observed, probably due to an extension of the anodic area responsible for corrosion. Nevertheless, from the value of current density, the thickness of the layer of corrosion products was estimated to be about 100  $\mu\text{m}$  after 24 h of contact between the disc and the NAO pad.

The EIS spectra of a disc alone and a disc coupled to pad samples performed at the corrosion potential after 150 min of immersion are presented in Fig. 5. In the case of the disc alone and the disc with the ceramic pad, both impedance spectra are similar in shape and amplitude. They show a capacitive behaviour with a large loop corresponding to the charge-transfer reaction in parallel with the interfacial capacitance. The low frequency limit of the impedance assimilated to the extrapolation to the real axis allows the polarization resistance,  $R_p$ , to be determined at *ca* 11  $\text{k}\Omega \text{ cm}^2$ , whereas from the characteristic frequency of the loop (*i.e.*  $f = 20 \text{ mHz}$ ) the interfacial capacitance was about 700  $\mu\text{F cm}^{-2}$ , which is one order of magnitude larger than the value expected for a double layer capacitance and at least two orders of magnitude larger than the value expected for a thin passive film. It is therefore to be ascribed to the response of the corrosion products possibly involving redox and/or ions exchange with the solution. The high concentration in Mn of the material (Table1), an element with many redox equilibria between its oxides is in favour of this interpretation. For these two cases involving either the disc alone and the disc with the ceramic pad, the shape of the EIS diagrams measured at the corrosion potential compares favourably with the results obtained on carbon steel in neutral sodium chloride solution (NaCl 3%) using a rotating disc electrode [41] as well as the EIS diagrams reported for cast iron in sea water [42].

When the system consisted in a cast iron disc and a NAO pad, the EIS spectrum is significantly different (Fig. 5 – blue curve). The overall magnitude of the diagrams is smaller and the EIS

1 response shows two time-constants: one capacitive loop in the high frequency domain and an  
2 inductive time-constant in the low frequency domain. The high frequency behaviour was  
3 ascribed to the charge-transfer reaction in parallel with the interfacial capacitance. It is worth  
4 noting that the charge transfer resistance is a direct measurement of the electron transfer rate,  
5 whereas the low frequency contribution (the inductive component in this case) can ascribed to  
6 the kinetically delayed phenomena involved in the whole electrochemical process. The  
7 resistance value was *ca.* 3000  $\Omega \text{ cm}^2$ , that is 3.5 times smaller than in absence of a pad or with  
8 a ceramic pad. This indicate an increase of the corrosion current density, in agreement with the  
9 analysis of the polarization curves. The characteristic frequency (240 mHz) allows a  
10 capacitance of *ca.* 250  $\mu\text{F cm}^{-2}$  to be determined. This value is still too large for being ascribed  
11 to a double layer capacitance or to the capacitance of a passive film. Since the cell geometry  
12 remained similar to the configuration with a ceramic pad, such a discrepancy must be ascribed  
13 to the nominal composition of the pad, the attention was thus focused on Cu. However, it is  
14 worth mentioning that corrosion products and copper deposit accumulate at the cast iron surface  
15 under the pad preferably, as shown on the optical observation of the disc presented in Fig. 8a.  
16 Thus, the true active area in that case is related to the area not screened by the pad rather than  
17 to the total area of the disc. This results in a decrease of the actual value of the charge transfer  
18 resistance (and thus an increase of the corrosion current density) and an increase of the  
19 interfacial capacitance, in agreement with an increase amount of electroactive corrosion  
20 products. However, it should also be noted that the geometric aspect alone is not necessarily  
21 sufficient to explain its variation and the kinetic aspect should not be neglected.

22 Additionally, the low frequency inductive loop can be ascribed to the relaxation of an adsorbed  
23 intermediate due the active dissolution of iron as discussed in [43,44].

1 At this point, the combination of the thin layer geometry and the presence of copper fibers in  
2 the pad significantly modify the electrochemical behaviour of the disc, whereas a chemically  
3 inert ceramic pad does not cause almost any influence on the corrosion rate of the disc.  
4

5  
6 However, for longer immersion times the EIS responses clearly show different behaviour of the  
7 whole system (Fig. 6). In fact, the impedance of the disc alone increases with time showing a  
8 progressive decrease of the corrosion rate while in the presence of a pad, the resistance of the  
9 system decreases with time before stabilizing. Moreover, the resistance value is lower for the  
10 NAO pad (Fig. 6c) than for the ceramic pad (Fig. 6b), thus showing that there is a thin layer  
11 effect on the corrosion behaviour of the braking system and the presence of copper is  
12 detrimental with respect to the corrosion rate.  
13  
14

15  
16 **Error! Reference source not found.** shows the evolution of the polarization resistance as a  
17 function of time for a single disc and a disc with a ceramic pad. These polarization resistance  
18 values were obtained by extrapolation at zero frequency from the impedance diagrams  
19 measured in 5% NaCl at the corrosion potential. The inverse of these values can be interpreted  
20 as a measure of the corrosion rate at each instant and shows that the bare disc has a corrosion  
21 rate that progressively decreases with time while the disc + ceramic pad system stabilizes after  
22 about 20 hours at a higher corrosion rate. It should also be noticed that during the first hours of  
23 immersion, both systems behave similarly, in agreement with the evolution of the corrosion  
24 potential presented in Fig. 3b. The higher corrosion of the disc below the ceramic pad in  
25 comparison to the bare disc can be attributed to the current and potential distribution in the thin-  
26 film configuration which will result in an increasing potential difference over time between  
27 different areas on the surface of the disc similarly to crevice corrosion.  
28  
29

### 30 3.2. Characterization of the corrosion products

31  
32 **Error! Reference source not found.** shows the optical image of the interface and a typical  
33 Raman spectrum acquired on a grain deposited at the surface after 72 h of immersion at the  
34  
35

1 OCP. The duration of the experiment was longer than the previous one in order to accumulate  
2 corrosion products at the interface. Additionally, to iron oxides coming from the oxidation of  
3  
4 the disc, metallic copper and copper oxides were evidenced. Most of the copper deposit was in  
5  
6 form of well faceted micro-crystals metallic copper (evidenced by EDAX analysis and the red  
7  
8 characteristic color of the metal), but from place to place, Raman spectrum (Fig. 8c) clearly  
9  
10 shows the presence of CuO and Cu<sub>2</sub>O [45,46]. Since the disc contains a negligible amount of  
11  
12 copper, this element can only come from the pad. The crystalline shapes exclude any  
13  
14 tribological transfer from the pad. In other words, the copper has first to dissolve from the pad  
15  
16 and then to deposit on the facing cast iron disc.  
17  
18  
19  
20  
21

22 In order to evidence this transfer mechanism of copper from the pad to the disc, experiment  
23  
24 with Teflon pad in which pure copper wires were inserted were performed in thin layer  
25  
26 configuration. Two different configurations were used, one with a single copper wire, the other  
27  
28 with 5 copper wires. In addition, in order to avoid any possible short-circuit between the  
29  
30 materials, 1 mm thick spacer were inserted between the pad and the disc. Figure S2 shows the  
31  
32 evolution of the OCP for the cast iron disc (black curve) and for the copper wire (red curve).  
33  
34 The copper electrode potential reaches a steady-state value of  $-0.210$  V *vs.* Ag/AgCl, whereas  
35  
36 the disc electrode reaches  $-0.770$  V *vs.* Ag/AgCl after 150 min of immersion in 5% NaCl  
37  
38 solution. When the same experiment is carried out with 5 copper wires in the Teflon pad, the  
39  
40 potentials of the copper electrodes are between  $-0.150$  and  $-0.210$  V *vs.* Ag/AgCl. Optical  
41  
42 microscopic observations of the disc surface after the experiment (Fig. S3) reveal a copper  
43  
44 deposit on the iron in front of each Cu electrode. The presence of this deposit is confirmed by  
45  
46 the EDAX analysis (Fig. S3c).  
47  
48  
49  
50  
51  
52  
53

### 54 3.3. Proposed mechanism 55 56 57 58 59 60 61 62 63 64 65

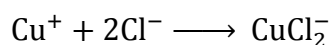
1 The electrodisolution of copper in chloride media was studied by several authors. Kear *et al.*  
2 made a critical review [47]. According to Bianchi *et al.* [48]  $\text{CuCl}_2^-$  is the main cuprous chloride  
3 complex in seawater and concentrated NaCl electrolytes, which is in agreement with most of  
4 the authors [49-52].  
5  
6  
7  
8  
9

10 **Error! Reference source not found.**a shows the variation of the potential with the cologarithm  
11 of the chloride concentration (pCl), so-called *E*-pCl diagram, plotted for two concentrations of  
12  $\text{Cu}^{2+}$  ( $10^{-3}$  M and  $10^{-5}$  M). For a concentration as low as  $10^{-5}$  M  $\text{Cu}^{2+}$ , at a potential close to 0  
13 V *vs.* SHE (corresponding to  $-0.200$  V *vs.* Ag/AgCl) and for a chloride concentration of 5%,  
14 we observe a dissolution of Cu into  $\text{CuCl}_2^-$ . This diagram also shows that for more negative  
15 potentials, a copper deposit can be observed. As a result, the copper may redeposit on the cast  
16 iron.  
17  
18  
19  
20  
21  
22  
23  
24  
25  
26

27 The Pourbaix diagram presented in Fig. 9b shows that the main species which form at neutral  
28 pH and for potential below 0 V *vs.* SHE is metallic copper, in agreement with our observation.  
29  
30  
31  
32

33 Thus, the following mechanism in the thin layer is proposed (Fig. 10):  
34  
35

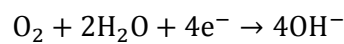
36 - The Cu wire is not contacting the disc so the potentials, OCP or other, measured on the disc –  
37  $0.770$  V *vs.* Ag/AgCl), does not apply to copper but to the cast iron alone. Copper corrodes  
38 independently of the cast iron at the expense of the oxygen present in the layer. It generates  
39 dissolved corrosion products through the reaction  
40  
41  
42  
43  
44  
45



50 After diffusion from the pad to the disc, cast iron potential is cathodic enough to reduce the  
51 cuprous ions into the metallic copper forming microcrystals as shown on the SEM and optical  
52 observations. This cathodic reaction is balanced for by the oxidation of the cast iron. We can  
53 predict that this corrosion would be circumscribed in the immediate vicinity of the redeposited  
54 Cu, but given the high conductivity of the medium it can also be located at remote sites but  
55  
56  
57  
58  
59  
60  
61  
62  
63  
64  
65

1 more sensitive to anodic dissolution. The distribution of Cu fibers is quite heterogeneous in the  
2 NAO pad. Nevertheless, an image analysis allows to estimate their number at about 300 fiber  
3 sections / cm<sup>2</sup>. Their section being between 100 and 200 μm in diameter (depending on their  
4 orientation in the pad), this represents 5 to 6% of the exposed pad surface.  
5  
6  
7

8  
9  
10 Overall, the transfer of copper facilitates the corrosion of the cast iron. Additionally, a direct  
11 contact between copper sites in the pad and cast iron can, by galvanic coupling, lead to the same  
12 effect as the graphite. Indeed, the presence of copper and copper oxides deposited in the form  
13 of microparticles on the steel substrate catalyses the cathodic oxygen reduction reaction [34,35],  
14 which is, in this neutral pH condition, given by  
15  
16  
17  
18  
19  
20  
21



23  
24  
25  
26 At corrosion potential, this reaction thus promotes the dissolution of iron by galvanic coupling.  
27  
28 It should be noted, however, that the thin-film configuration limits the oxygen supply, thereby  
29 minimizing the detrimental effect of copper and its oxides on the corrosion of the brake disc.  
30  
31 On the other hand, the potential gradient inside the thin layer combined to the local pH change  
32 in it, may results in proton reduction as cathodic reaction after the consumption of dissolved  
33 O<sub>2</sub>. This is in agreement with the increase of the corrosion current density observed on the  
34 polarization curves (Fig. 4) and the EIS analysis (Fig. 5). Moreover, the pH in the thin-layer  
35 may also significantly vary due to the different reaction occurring inside such a small volume.  
36  
37 This can also modify the reactivity inside the thin layer, including the oxygen reduction reaction  
38 and the formation of iron complexes with hydroxide ions.  
39  
40  
41  
42  
43  
44  
45  
46  
47  
48  
49  
50  
51  
52  
53  
54

## 55 4. Conclusions

56  
57  
58  
59  
60  
61  
62  
63  
64  
65

1 This work presented the study of a brake system under a thin-film corrosion perspective. We  
2 showed that the corrosion of such a system, i.e. is a steel disk facing a copper containing  
3 material, can be exacerbated but that the thin-film configuration alone does not appear to be  
4 sufficient to alter the current and potential distribution in the thin electrolyte volume and explain  
5 an increase in the corrosion rate of the steel disk for short immersion times (less than 20 hours).  
6  
7 For longer immersion time performed on a thin-film configuration involving a steel disk and a  
8 ceramic pad, a significant shift of corrosion potential was observed together with an increase  
9 of the corrosion current density. Moreover, it has been shown that the presence of the second  
10 material, namely the copper fibers contains in the pad, is detrimental to the system. The different  
11 electrochemical techniques used have shown a correlation between the measured  
12 electrochemical responses and the nature of the brake pads, thus indicating a concomitant effect  
13 of the geometry of the system and the chemistry inside the thin layer.  
14  
15  
16  
17  
18  
19  
20  
21  
22  
23  
24  
25  
26  
27  
28

29 A model taking into account the dissolution of the copper contained in the pad that redeposits  
30 on the disc has been proposed. It shows that the potential of the steel disk is cathodic enough to  
31 enable the redeposition of copper resulting from the dissolution of the fibers of the pad. Such a  
32 description is in agreement with the thermodynamic conditions of the system and also helps to  
33 explain the increase in corrosion current density.  
34  
35  
36  
37  
38  
39  
40  
41  
42  
43  
44

## 45 5. Acknowledgements

46 Rafik Tigane gratefully acknowledges Hitachi Automotive Systems and CNRS for financial  
47 support.  
48  
49  
50  
51  
52  
53  
54  
55  
56  
57  
58  
59  
60  
61  
62  
63  
64  
65

## 6. References

1. Rashid A (2014) Overview of disc brakes and related phenomena - a review. *International Journal of Vehicle Noise and Vibration* 10 (4):257-301. doi:10.1504/ijvnnv.2014.065634
2. Li WY, Yang XF, Wang SR, Xiao JP, Hou QM (2020) Comprehensive Analysis on the Performance and Material of Automobile Brake Discs. *Metals* 10 (3). doi:ARTN 377  
10.3390/met10030377
3. Österle W, Prietzel C, Kloß H, Dmitriev AI (2010) On the role of copper in brake friction materials. *Tribology International* 43 (12):2317-2326. doi:10.1016/j.triboint.2010.08.005
4. Kumar M, Bijwe J (2011) Non-asbestos organic (NAO) friction composites: Role of copper; its shape and amount. *Wear* 270 (3-4):269-280. doi:10.1016/j.wear.2010.10.068
5. Sanders PG, Xu N, Dalka TM, Maricq MM (2003) Airborne brake wear debris: size distributions, composition, and a comparison of dynamometer and vehicle tests. *Environ Sci Technol* 37 (18):4060-4069. doi:10.1021/es034145s
6. Robere M (2016) Disc Brake Pad Corrosion Adhesion: Test-to-Field Issue Correlation, and Exploration of Friction Physical Properties Influence to Adhesion Break-Away Force. Paper presented at the SAE Technical Paper Series, 2016-09-18
7. Passarelli UP, Merlo F, Pellerej D, Buonficio P (2012) Influence of Brake Pad Porosity and Hydrophilicity on Stiction by Corrosion of Friction Material against Gray Cast Iron Rotor. Paper presented at the SAE Technical Paper Series, 2012-09-17
8. Gweon J, Shin S, Jang H, Lee W, Kim D, Lee K (2018) The Factors Governing Corrosion Stiction of Brake Friction Materials to a Gray Cast Iron Disc. Paper presented at the SAE Technical Paper Series, 2018-10-05
9. Rosenfeld IL, Marshakov IK (1964) Mechanism of Crevice Corrosion. *Corrosion* 20 (4):115t-125t. doi:10.5006/0010-9312-20.4.115t
10. Wolfe RC, Weil KG, Pickering HW (2004) Electrochemical Probes for Metal/Electrolyte System Characterization during Crevice Corrosion†. *J Phys Chem B* 108 (38):14298-14304. doi:10.1021/jp040045c
11. Pickering HW (2007) IR Voltage in Crevices during Crevice Corrosion and Sacrificial Cathodic Protection. *Zeitschrift für Physikalische Chemie* 221 (11-12):1441-1454. doi:10.1524/zpch.2007.221.11-12.1441
12. Kennell GF, Evitts RW (2009) Crevice corrosion cathodic reactions and crevice scaling laws. *Electrochim Acta* 54 (20):4696-4703. doi:10.1016/j.electacta.2009.03.080

- 1  
2  
3  
4  
5  
6  
7  
8  
9  
10  
11  
12  
13  
14  
15  
16  
17  
18  
19  
20  
21  
22  
23  
24  
25  
26  
27  
28  
29  
30  
31  
32  
33  
34  
35  
36  
37  
38  
39  
40  
41  
42  
43  
44  
45  
46  
47  
48  
49  
50  
51  
52  
53  
54  
55  
56  
57  
58  
59  
60  
61  
62  
63  
64  
65
13. Aoyama T, Sugawara Y, Muto I, Hara N (2017) In situ monitoring of crevice corrosion morphology of Type 316L stainless steel and repassivation behavior induced by sulfate ions. *Corros Sci* 127:131-140. doi:10.1016/j.corsci.2017.08.005
  14. Pickering HW, Beck FH, Fontana MG (1962) Wedging Action of Solid Corrosion Product During Stress Corrosion of Austenitic Stainless Steels. *Corrosion* 18 (6):230t-239t. doi:10.5006/0010-9312-18.6.230
  15. Shahidzadeh N, Desarnaud J (2012) Damage in porous media: role of the kinetics of salt (re)crystallization. *Eur Phys J Appl Phys* 60 (2)
  16. Desarnaud J, Bonn D, Shahidzadeh N (2016) The Pressure induced by salt crystallization in confinement. *Sci Rep* 6 (1):30856. doi:10.1038/srep30856
  17. Dante RC (2016) Types of friction material formulas. In: Dante RC (ed) *Handbook of Friction Materials and their Applications*. Woodhead Publishing, Boston, pp 29-54. doi:10.1016/b978-0-08-100619-1.00003-1
  18. Xiao P, Li ZA, Xiong X (2010) Microstructure and tribological properties of 3D needle-punched C/C-SiC brake composites. *Solid State Sciences* 12 (4):617-623. doi:10.1016/j.solidstatesciences.2010.01.014
  19. Kumar M, Bijwe J (2010) Role of different metallic fillers in non-asbestos organic (NAO) friction composites for controlling sensitivity of coefficient of friction to load and speed. *Tribology International* 43 (5-6):965-974. doi:10.1016/j.triboint.2009.12.062
  20. Djafri M, Bouchetara M, Busch C, Weber S (2014) Effects of humidity and corrosion on the tribological behaviour of the brake disc materials. *Wear* 321:8-15. doi:10.1016/j.wear.2014.09.006
  21. Mirzababaei S, Filip P (2017) Impact of humidity on wear of automotive friction materials. *Wear* 376:717-726. doi:10.1016/j.wear.2017.02.020
  22. Blau PJ, Truhan JJ, Kenik EA (2007) Effects of the exposure to corrosive salts on the frictional behavior of gray cast iron and a titanium-based metal matrix composite. *Tribology International* 40 (9):1335-1343. doi:10.1016/j.triboint.2007.02.020
  23. Nukumizu K, Makizono K, Abe T, Unno M (2007) Influence of Rust Accumulation on Disk Rotor on Frictional Properties of Disk Brake. Paper presented at the SAE Technical Paper Series, 2007-10-07
  24. Leonardi M, Menapace C, Matejka V, Gialanella S, Straffelini G (2018) Pin-on-disc investigation on copper-free friction materials dry sliding against cast iron. *Tribology International* 119:73-81. doi:10.1016/j.triboint.2017.10.037

- 1  
2  
3  
4  
5  
6  
7  
8  
9  
10  
11  
12  
13  
14  
15  
16  
17  
18  
19  
20  
21  
22  
23  
24  
25  
26  
27  
28  
29  
30  
31  
32  
33  
34  
35  
36  
37  
38  
39  
40  
41  
42  
43  
44  
45  
46  
47  
48  
49  
50  
51  
52  
53  
54  
55  
56  
57  
58  
59  
60  
61  
62  
63  
64  
65
25. Park CW, Shin MW, Jang H (2014) Friction-induced stick-slip intensified by corrosion of gray iron brake disc. *Wear* 309 (1-2):89-95. doi:10.1016/j.wear.2013.11.008
  26. Cho KH, Han JM, Jang H, Kim SJ, Lee JY, Park HD, Oh JS, Lim JD (2005) Corrosion Induced Brake Torque Variation: The Effect from Gray Iron Microstructure and Friction Materials. Paper presented at the SAE Technical Paper Series, 2005-10-09
  27. Fiaud C, Keddad M, Kadri A, Takenouti H (1987) Electrochemical Impedance in a Thin Surface Electrolyte Layer - Influence of the Potential Probe Location. *Electrochim Acta* 32 (3):445-448. doi:Doi 10.1016/0013-4686(87)85011-9
  28. Remita E, Bouhrara A, Tribollet B, Vivier V, Sutter E, Ropital F, Kittel J (2008) Diffusion impedance in a thin-layer cell: Experimental and theoretical study on a large-disk electrode. *Journal of Physical Chemistry C* 112 (12):4626-4634. doi:10.1021/jp710407a
  29. Dante RC (2016) Metals. In: *Handbook of Friction Materials and their Applications*. pp 123-134. doi:10.1016/b978-0-08-100619-1.00009-2
  30. Österle W, Urban I (2004) Friction layers and friction films on PMC brake pads. *Wear* 257 (1-2):215-226. doi:10.1016/j.wear.2003.12.017
  31. Federici M, Gialanella S, Leonardi M, Perricone G, Straffelini G (2018) A preliminary investigation on the use of the pin-on-disc test to simulate off-brake friction and wear characteristics of friction materials. *Wear* 410:202-209. doi:10.1016/j.wear.2018.07.011
  32. Chandra Verma P, Menapace L, Bonfanti A, Ciudin R, Gialanella S, Straffelini G (2015) Braking pad-disc system: Wear mechanisms and formation of wear fragments. *Wear* 322-323:251-258. doi:10.1016/j.wear.2014.11.019
  33. Dante RC (2016) Friction materials. In: Dante RC (ed) *Handbook of Friction Materials and their Applications*. Woodhead Publishing, Boston, pp 1-6. doi:10.1016/b978-0-08-100619-1.00001-8
  34. King F, Quinn MJ, Litke CD (1995) Oxygen Reduction on Copper in Neutral NaCl Solution. *J Electroanal Chem* 385 (1):45-55. doi:Doi 10.1016/0022-0728(94)03705-8
  35. Li F, Han GF, Noh HJ, Kim SJ, Lu YL, Jeong HY, Fu ZP, Baek JB (2018) Boosting oxygen reduction catalysis with abundant copper single atom active sites. *Energy & Environmental Science* 11 (8):2263-2269. doi:10.1039/c8ee01169a
  36. Santos DMF, Sequeira CAC, Figueiredo JL (2013) Hydrogen Production by Alkaline Water Electrolysis. *Quimica Nova* 36 (8):1176-1193. doi:Doi 10.1590/S0100-40422013000800017

- 1  
2  
3  
4  
5  
6  
7  
8  
9  
10  
11  
12  
13  
14  
15  
16  
17  
18  
19  
20  
21  
22  
23  
24  
25  
26  
27  
28  
29  
30  
31  
32  
33  
34  
35  
36  
37  
38  
39  
40  
41  
42  
43  
44  
45  
46  
47  
48  
49  
50  
51  
52  
53  
54  
55  
56  
57  
58  
59  
60  
61  
62  
63  
64  
65
37. Ooka H, Figueiredo MC, Koper MTM (2017) Competition between Hydrogen Evolution and Carbon Dioxide Reduction on Copper Electrodes in Mildly Acidic Media. *Langmuir* 33 (37):9307-9313. doi:10.1021/acs.langmuir.7b00696
38. Bonnel A, Dabosi F, Deslouis C, Duprat M, Keddam M, Tribollet B (2019) Response to “Comment on ‘Corrosion Study of a Carbon Steel in Neutral Chloride Solution by Impedance Techniques’” [*J. Electrochem. Soc.*, 130, 753]. *J Electrochem Soc* 132 (1):256-256. doi:10.1149/1.2148671
39. Lantiat D, Vivier V, Laberty-Robert C, Grosso D, Sanchez C (2010) Gold Nanoelectrode Arrays and their Evaluation by Impedance Spectroscopy and Cyclic Voltammetry. *Chemphyschem* 11 (9):1971-1977. doi:10.1002/cphc.200900929
40. Caprani A, Deslouis C, Keddam M, Morel P, Tribollet B (1977) Study of Partially Blocked Electrodes by Means of Electromechanical Impedance Measurements. *Electrochim Acta* 22 (11):1231-1235. doi:Doi 10.1016/0013-4686(77)87001-1
41. Bonnel A, Dabosi F, Deslouis C, Duprat M, Keddam M, Tribollet B (1983) Corrosion Study of a Carbon-Steel in Neutral Chloride Solutions by Impedance Techniques. *J Electrochem Soc* 130 (4):753-761. doi:Doi 10.1149/1.2119798
42. Song Y, Jiang G, Chen Y, Zhao P, Tian Y (2017) Effects of chloride ions on corrosion of ductile iron and carbon steel in soil environments. *Sci Rep* 7 (1):6865. doi:10.1038/s41598-017-07245-1
43. Keddam M, Mattos OR, Takenouti H (2019) Reaction Model for Iron Dissolution Studied by Electrode Impedance: II . Determination of the Reaction Model. *J Electrochem Soc* 128 (2):266-274. doi:10.1149/1.2127402
44. Keddam M, Mottos OR, Takenouti H (2019) Reaction Model for Iron Dissolution Studied by Electrode Impedance: I . Experimental Results and Reaction Model. *J Electrochem Soc* 128 (2):257-266. doi:10.1149/1.2127401
45. Debbichi L, de Lucas MCM, Pierson JF, Kruger P (2012) Vibrational Properties of CuO and Cu<sub>4</sub>O<sub>3</sub> from First-Principles Calculations, and Raman and Infrared Spectroscopy. *Journal of Physical Chemistry C* 116 (18):10232-10237. doi:10.1021/jp303096m
46. Bouchard M, Smith DC (2003) Catalogue of 45 reference Raman spectra of minerals concerning research in art history or archaeology, especially on corroded metals and coloured glass. *Spectrochimica Acta Part a-Molecular and Biomolecular Spectroscopy* 59 (10):2247-2266. doi:10.1016/S1386-1425(03)00069-6

- 1  
2  
3  
4  
5  
6  
7  
8  
9  
10  
11  
12  
13  
14  
15  
16  
17  
18  
19  
20  
21  
22  
23  
24  
25  
26  
27  
28  
29  
30  
31  
32  
33  
34  
35  
36  
37  
38  
39  
40  
41  
42  
43  
44  
45  
46  
47  
48  
49  
50  
51  
52  
53  
54  
55  
56  
57  
58  
59  
60  
61  
62  
63  
64  
65
47. Kear G, Barker BD, Walsh FC (2004) Electrochemical corrosion of unalloyed copper in chloride media - a critical review. *Corros Sci* 46 (1):109-135. doi:10.1016/S0010-938x(02)00257-3
48. Bianchi G, Fiori G, Longhi P, Mazza F (1978) "Horse Shoe" Corrosion of Copper Alloys in Flowing Sea Water: Mechanism, and Possibility of Cathodic Protection of Condenser Tubes in Power Stations. *Corrosion* 34 (11):396-406. doi:10.5006/0010-9312-34.11.396
49. Deslouis C, Tribollet B, Mengoli G, Musiani MM (1988) Electrochemical behaviour of copper in neutral aerated chloride solution. II. Impedance investigation. *J Appl Electrochem* 18 (3):384-393. doi:10.1007/bf01093752
50. Deslouis C, Tribollet B, Mengoli G, Musiani MM (1988) Electrochemical behaviour of copper in neutral aerated chloride solution. I. Steady-state investigation. *J Appl Electrochem* 18 (3):374-383. doi:10.1007/bf01093751
51. Wood RJK, Hutton SP, Schiffrin DJ (1990) Mass transfer effects of non-cavitating seawater on the corrosion of Cu and 70Cu-30Ni. *Corros Sci* 30 (12):1177-1201. doi:10.1016/0010-938x(90)90198-e
52. Liao XN, Cao FH, Zheng LY, Liu WJ, Chen AN, Zhang JQ, Cao CA (2011) Corrosion behaviour of copper under chloride-containing thin electrolyte layer. *Corros Sci* 53 (10):3289-3298. doi:10.1016/j.corsci.2011.06.004

## Captions

**Table 1** – Chemical composition of disc samples in weight percent (wt%).

**Figure 1** – Brake disc sample (a) and brake pad sample (b)

**Figure 2** – Experimental set-up used for studying the corrosion of the disc/pad system in a thin layer configuration.

**Figure 3** – Variations of the corrosion potential in 5% NaCl solution as a function of time of the bare disc (black curve), in presence of ceramic (red curve) and NAO (blue curve) pads: (a) short immersion time; (b) long immersion time.

**Figure 4** – Quasi steady-state polarization curves measured in 5% NaCl solution at  $0.2 \text{ mVs}^{-1}$  with a bare disc (black curve), and in presence of ceramic (red curve) and NAO (blue curve) pads touching the surface. Dashed curves were measured after 10 min immersion at the corrosion potential and solid curves were measured after 150 min immersion at the corrosion potential.

**Figure 5** – EIS spectra in Nyquist format measured at the corrosion potential after 3 hours immersion in 5% NaCl solution of the bare disc, and in presence of ceramic or NAO pads.

**Figure 6** – EIS spectra in Nyquist format measured at the corrosion potential as a function of immersion time in 5% NaCl solution of the bare disc (a), and in presence of ceramic (b) or NAO (c) pads.

**Figure 7** – Evolution of the polarization resistance determined from EIS at the corrosion potential as a function of immersion time in 5% NaCl solution for the bare disc (dark circles), and in presence of a ceramic pad (red squares).

**Figure 8** – Optical observations of the sample at different magnifications (a) & (b); and Raman spectrum measured on a grain deposited on the disc under the pad (c) after 72 hours of immersion at the corrosion potential in 5% NaCl solution.

**Figure 9** – E – pCl (a) and E – pH (b) diagrams for copper

**Figure 10** – Mechanism of copper dissolution and redeposition at brake disc surface in a thin layer of electrolyte configuration



[Click here to access/download](#)

**Supplementary Material**

CBI Article Rafik final3-Rev1 - SM.docx

